Tobin, H., Hirose, T., Ikari, M., Kanagawa, K., Kimura, G., Kinoshita, M., Kitajima, H., Saffer, D., Yamaguchi, A., Eguchi, N., Maeda, L., Toczko, S., and the Expedition 358 Scientists Proceedings of the International Ocean Discovery Program Volume 358 publications.iodp.org



https://doi.org/10.14379/iodp.proc.358.101.2020



Expedition 358 summary¹

H. Tobin, T. Hirose, M. Ikari, K. Kanagawa, G. Kimura, M. Kinoshita, H. Kitajima, D. Saffer, A. Yamaguchi, N. Eguchi, L. Maeda, S. Toczko, J. Bedford, S. Chiyonobu, T.A. Colson, M. Conin, P.H. Cornard, A. Dielforder, M.-L. Doan, J. Dutilleul, D.R. Faulkner, R. Fukuchi, G. Guérin, Y. Hamada, M. Hamahashi, W.-L. Hong, A. Ijiri, D. Jaeger, T. Jeppson, Z. Jin, B.E. John, M. Kitamura, A. Kopf, H. Masuda, A. Matsuoka, G.F. Moore, M. Otsubo, C. Regalla, A. Sakaguchi, J. Sample, A. Schleicher, H. Sone, K. Stanislowski, M. Strasser, T. Toki, T. Tsuji, K. Ujiie, M.B. Underwood, S. Yabe, Y. Yamamoto, J. Zhang, Y. Sanada, Y. Kido, E. Le Ber, and S. Saito with contributions by T. Kanamatsu²

Keywords: International Ocean Discovery Program, IODP, Chikyu, Expedition 358, NanTroSEIZE Plate Boundary Deep Riser 4: Nankai Seismogenic/Slow Slip Megathrust, Site C0002, Site C0024, Site C0025, Kumano Basin, Nankai accretionary prism, frontal thrust, riser drilling, logging while drilling, LWD

Contents

- **Abstract**
- 2 Introduction and background
- 4 Principal results
- 13 Preliminary scientific assessment
- 14 References

Abstract

International Ocean Discovery Program (IODP) Expedition 358 was carried out from October 2018 through March 2019 on the D/V Chikyu in an attempt to reach a plate boundary fault zone at seismogenic depths for the first time in scientific ocean drilling. The goal was to extend Hole C0002P from ~2900 to ~5200 meters below seafloor (mbsf) and cross the seismically interpreted main décollement fault zone with logging while drilling, downhole stress measurements, cuttings sampling, mud gas sampling, and partial coring by drilling a sidetrack to create a new hole (C0002Q). Although drilling reached 3262.5 mbsf, the deepest to date in all of scientific ocean drilling, the effort to drill to and sample the target—the megathrust fault zone—was not successful. Operational challenges in establishing sidetrack holes and advancing them at reasonable rates of penetration limited the new cased hole interval to less than 60 m total at a depth shallower than the previously established casing depth of 2922 mbsf. Combined, the cuttings, logs, and ~60 cm of recovered core from sidetrack Holes C0002Q-C0002T revealed hemipelagic sediments and fine silty turbidites consistent in lithology and physical properties with those recovered in the same depth interval at the same site during Integrated Ocean Drilling Program Expedition 348. Cuttings revealed evidence of only weakly deformed rock, with relatively common calcite veins but few other structural indicators.

Because no downhole leak-off tests were made and very little borehole imaging was performed, no further insight into the tectonic context was acquired.

After riser drilling at Site C0002 was terminated, drilling at alternate contingency Sites C0024 and C0025 was carried out. Site C0024 targeted the frontal thrust region to sample and log hanging wall rocks and the shallow portion of the décollement zone, and Site C0025 accessed sediments in the Kumano fore-arc basin. At Site C0024, a dedicated logging hole was drilled and a very complete suite of logs were acquired from 0 to 869 mbsf. Preliminary interpretation of log response and images suggests the frontal thrust zone was encountered from about 813 mbsf to the base of the hole, with a zone of notably low resistivity and steep bedding from 850 mbsf to the bottom of the hole. Core samples revealed lithologic units interpreted to be hemipelagic and turbiditic basin fill, trench fill, and Shikoku Basin sediments and encountered deformation potentially associated with a back thrust imaged in seismic reflection data. However, coring had to be terminated at about 620 mbsf, well short of the frontal thrust zone. Site C0025 recovered fore-arc basin sediments underlain by those interpreted to have been deposited in a trench-slope basin setting; no clear transition into older, inner accretionary wedge material was identified during the preliminary analysis. Coring from 400 to 571 mbsf yielded datable material and possible evidence for diapiric intrusion of sediments.

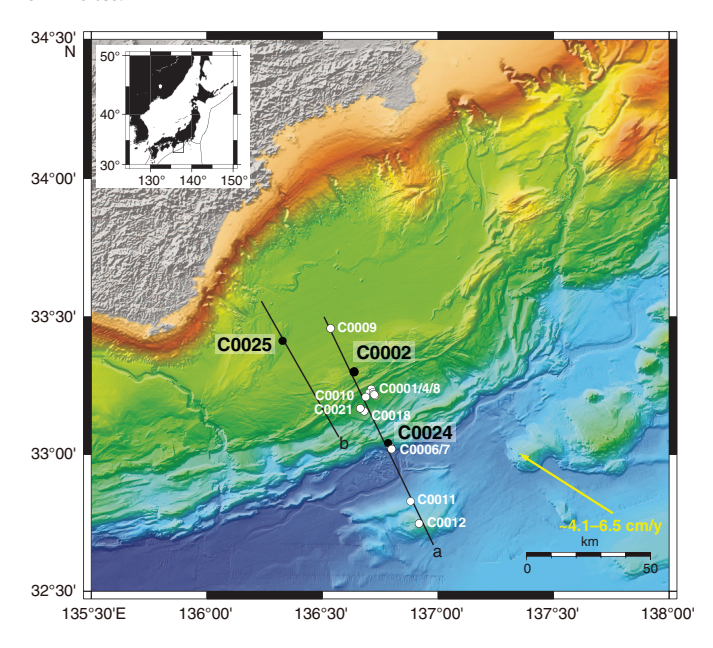
¹ Tobin, H., Hirose, T., Ikari, M., Kanagawa, K., Kimura, G., Kinoshita, M., Kitajima, H., Saffer, D., Yamaguchi, A., Eguchi, N., Maeda, L., Toczko, S., Bedford, J., Chiyonobu, S., Colson, T.A., Conin, M., Cornard, P.H., Dielforder, A., Doan, M.-L., Dutilleul, J., Faulkner, D.R., Fukuchi, R., Guérin, G., Hamada, Y., Hamahashi, M., Hong, W.-L., Ijiri, A., Jaeger, D., Jeppson, T., Jin, Z., John, B.E., Kitamura, M., Kopf, A., Masuda, H., Matsuoka, A., Moore, G.F., Otsubo, M., Regalla, C., Sakaguchi, A., Sample, J., Schleicher, A., Sone, H., Stanislowski, K., Strasser, M., Toki, T., Tsuji, T., Ujiie, K., Underwood, M.B., Yabe, S., Yamamoto, Y., Zhang, J., Sanada, Y., Kido, Y., Le Ber, E., and Saito, S., 2020. Expedition 358 summary. With contributions by T. Kanamatsu. In Tobin, H., Hirose, T., Ikari, M., Kanagawa, K., Kimura, G., Kinoshita, M., Kitajima, H., Saffer, D., Yamaguchi, A. Eguchi, N., Maeda, L., Toczko, S., and the Expedition 358 Scientists, NanTro-SEIZE Plate Boundary Deep Riser 4: Nankai Seismogenic/Slow Slip Megathrust. Proceedings of the International Ocean Discovery Program, 358: College Station, TX (International Ocean Discovery Program). https://doi.org/10.14379/iodp.proc.358.101.2020

² Expedition 358 Scientists' affiliations.

Introduction and background

The Nankai Trough Seismogenic Zone Experiment (NanTro-SEIZE) program is a coordinated, multiexpedition drilling project designed to investigate fault mechanics and seismogenesis along the Nankai subduction megathrust (Figure F1) through direct sampling, in situ measurements, and long-term monitoring in conjunction with allied laboratory and numerical modeling studies (Tobin and Kinoshita, 2006; Tobin et al., 2015a, 2019). The fundamental scientific objectives of the NanTroSEIZE project include characterizing the nature of fault slip and strain accumulation, fault and wall

Figure F1. NanTroSEIZE transect map. Transect Lines a and b refer to composite seismic depth section of Figure F2A and Line ODKM-B of Figure F2B, respectively. Solid dots = Expedition 358 sites, open dots = previous NanTro-SEIZE sites.



rock composition, fault architecture, and state variables throughout the active plate boundary system. Eleven previous expeditions have established a transect of sites from the incoming (subducting) plate through fault zone and accretionary wedge characterization and into the central fore-arc basin (Figure F2). For reviews of many of the principal results from these sites, see Underwood and Moore (2012), Ujiie and Kimura (2014), and Tobin et al. (2015b, 2019).

Site C0002 is located in the Kumano fore-arc basin above the seismogenic, partially locked portion of the plate boundary thrust system (Figures F1, F2, F3). The Kumano Basin sedimentary sequence and uppermost part of the accretionary prism were drilled, logged, and sampled during Integrated Ocean Drilling Program Expeditions 314 (logging while drilling [LWD] to 1401.5 meters below seafloor [mbsf]), 315 (coring to 1057 mbsf), 338 (LWD to 2005 mbsf and coring to 1120 mbsf), and 348 (LWD to 3058.5 mbsf, with limited coring from 2163 to 2218.5 mbsf) (Expedition 314 Scientists, 2009; Expedition 315 Scientists, 2009; Strasser et al., 2014; Tobin et al., 2015b).

The principal goal of International Ocean Discovery Program (IODP) Expedition 358 was to reach and sample the reflector identified as the likely plate boundary fault at Site C0002 by extending the riser borehole (Hole C0002P) established during previous Integrated Ocean Drilling Program NanTroSEIZE expeditions (Figure F3). This drilling target is also in close proximity to the location of very low frequency (VLF) earthquakes and the first tectonic tremor recorded in any accretionary prism setting (summarized in Obara and Kato, 2016), all of which suggest that fault processes related to the updip limit of megathrust seismogenic mechanics are active here. Recent results from the NanTroSEIZE long-term borehole monitoring systems and Dense Oceanfloor Network System for Earthquakes and Tsunamis (DONET) seafloor observations further suggest that the plate boundary at this location is partially locked and partially releasing plate convergence strain in these slow slip events accompanied by low-frequency tectonic tremor and VLF earthquakes (Araki et al., 2017).

A detailed drilling plan was developed by the Center for Deep Earth Exploration after careful analyses of the Expedition 338 and

Figure F2. A. Regional seismic reflection depth-processed imaging for Sites C0002 and C0024 and other previously drilled NanTroSEIZE sites. BSR = bottom-simulating reflector, PTZ = protothrust zone. B. Japan Agency for Marine-Earth Science and Technology Seismic Reflection Line ODKM-B showing location of Site C0025. Blue circles = interpreted boundary between Kumano fore-arc basin sediments and underlying inner accretionary prism, white circles = interpreted depths of splay fault branching from plate boundary.

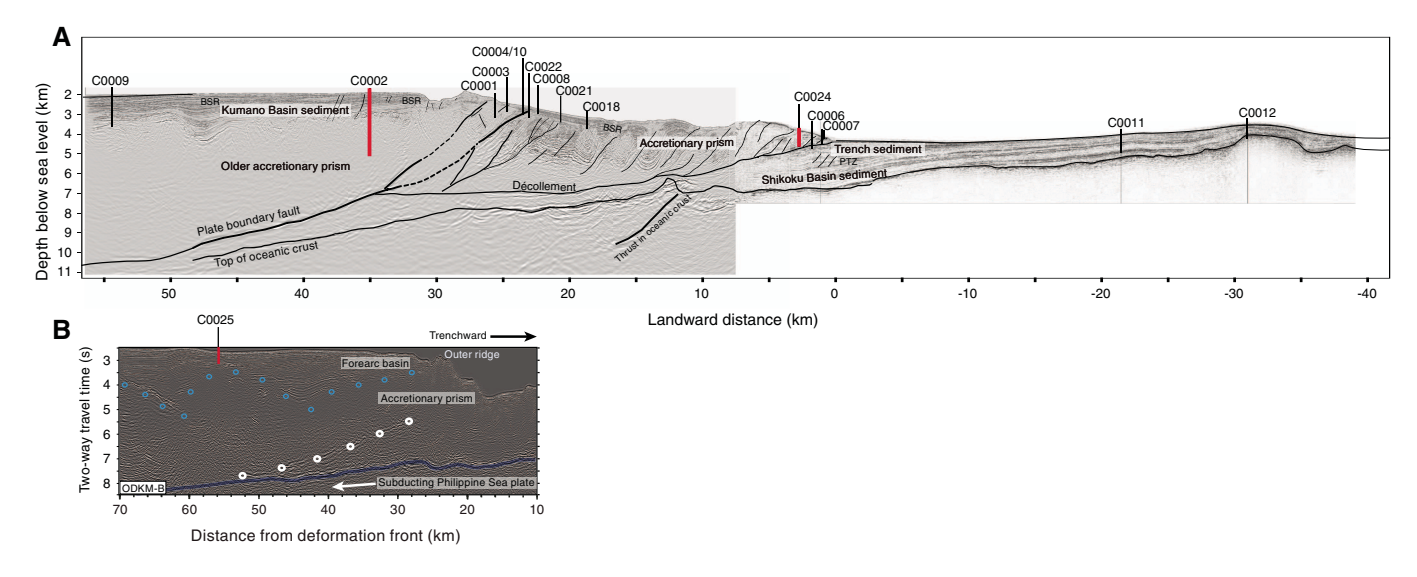
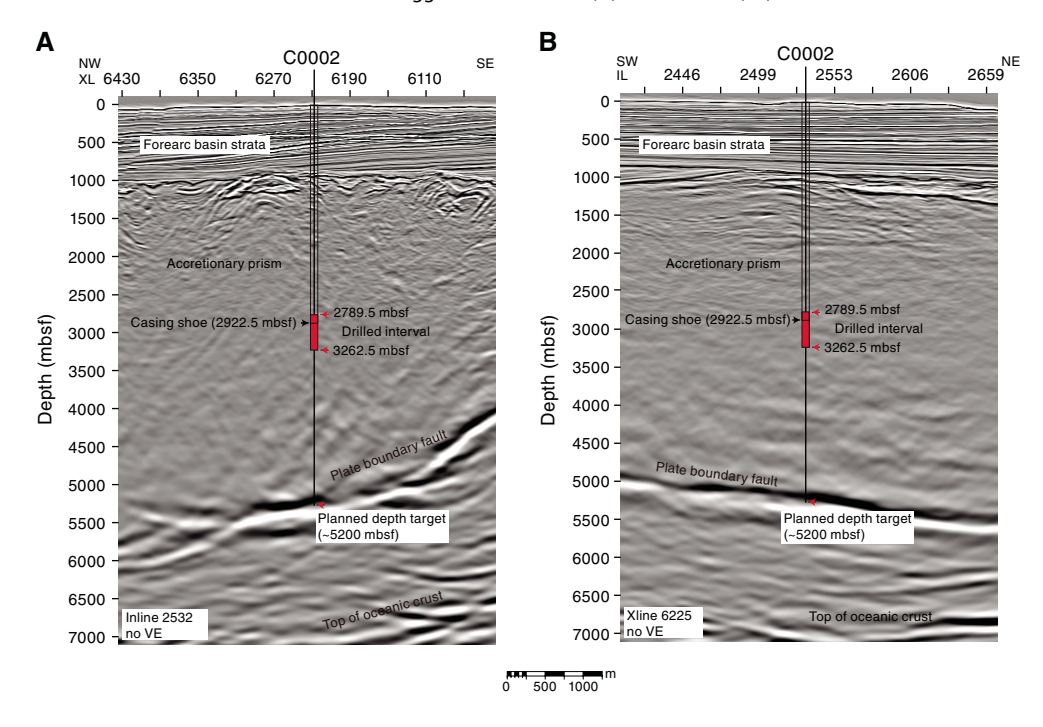


Figure F3. Seismic cross sections near Site C0002. VE = vertical exaggeration. A. In-line (IL). B. Cross-line (XL).



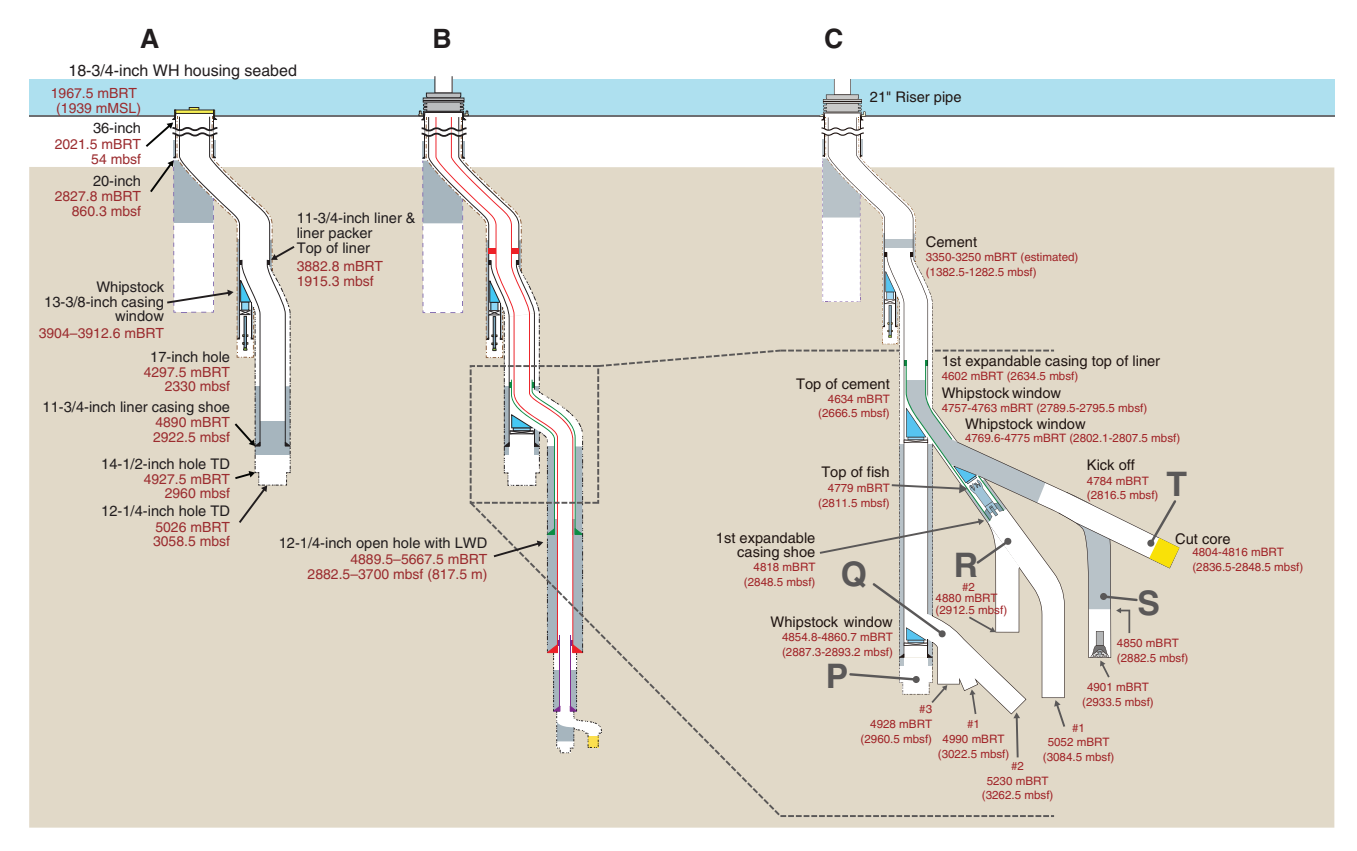
348 drilling experiences (Figure F4). It involved sidetracking from near the bottom of the Hole C0002P casing pipe at 2880 mbsf to begin Hole C0002Q and then advancing in three casing stages, alternately drilling and then cementing in successive casing strings to reach the zone just ~200 m above the anticipated plate boundary fault zone. A comprehensive suite of LWD measurements were planned, along with detailed cuttings analysis, to monitor progress and characterize the lower accretionary wedge/hanging wall of the fault zone. The final stage of operations was planned to drill across the high-amplitude seismic reflector identified as the main plate boundary fault zone with LWD and then drill an open hole sidetrack for a second pass to core 100–200 m in total from the hanging wall across the fault and into the footwall (Figure F4).

For the ~2000 m interval of planned drilling above the target zone, the primary scientific objectives were to (1) determine the composition, stratigraphy, and deformational history of the Miocene accretionary wedge; (2) reconstruct its thermal, diagenetic,

and metamorphic history; (3) determine horizontal stress orientations and magnitudes; and (4) investigate the mechanical and hydrological properties of the upper plate of the seismogenic plate boundary. In the target zone, comprehensive structural, lithologic/petrologic, and physical property characterization of the fault zone and wall rocks was planned using cuttings, logging, and continuous core sampling. The final objective was to leave the borehole in a condition that would allow for design and deployment of a long-term in situ borehole observatory system subsequent to the expedition.

Previous major riser drilling efforts during Expeditions 338 and 348 advanced the main riser hole at Site C0002 (Holes C0002F, C0002N, and C0002P) to 3058.5 mbsf, and casing was installed in that hole to 2922.5 mbsf (Figures **F3**, **F4A**). Extensive downhole logging data, continuously sampled drill cuttings, and limited intervals of core were collected during those expeditions.

Figure F4. Schematic diagrams (not to scale). Horizontal black line between blue and white bands = seafloor. A. Holes C0002F/C0002N/C0002P drilled during previous expeditions. WH = wellhead. BRT = below rotary table, MSL = from mean sea level. TD = total depth. B. Expedition 358 drilling and casing plan, building downward from preexisting Hole C0002P. LWD = logging while drilling. C. Actual holes drilled during Expedition 358. Note the change in relative scale compared to A and B.



Principal results

Site C0002

Summary of planned Site C0002 riser operations for Expedition 358:

- Employ the riser drilling technique, kick off from at or above the existing 11% inch casing shoe at 2922.5 mbsf and open a new hole to $\sim\!5200$ mbsf or the maximum achievable depth within time and budget limits, setting 9% inch (expanded to 11% inch) casing, 9% inch steel liner, and 7% inch (expanded to 9% inch) casing to $\sim\!4700$ mbsf and open hole drilling with an 8% inch diameter bit below that to total depth (TD).
- Use a suite of LWD/measurement-while-drilling tools and measurements to include gamma ray, sonic, and resistivity logs and images. Analyze lithology, physical properties, and geochemistry of cuttings from the entire drilled interval at a suitable spacing (nominally every 10 m).
- At casing set points and other opportunities, conduct downhole tests—formation integrity test, extended leak-off tests (XLOTs), leak-off tests (LOTs), and other formation tests—to evaluate in situ stress, pore fluid pressure, permeability, and rock strength conditions.
- Core about 100 m: ~50 m from 4650 mbsf and ~50 m from 5150 mbsf or at a depth selected as we penetrate the fault zone.

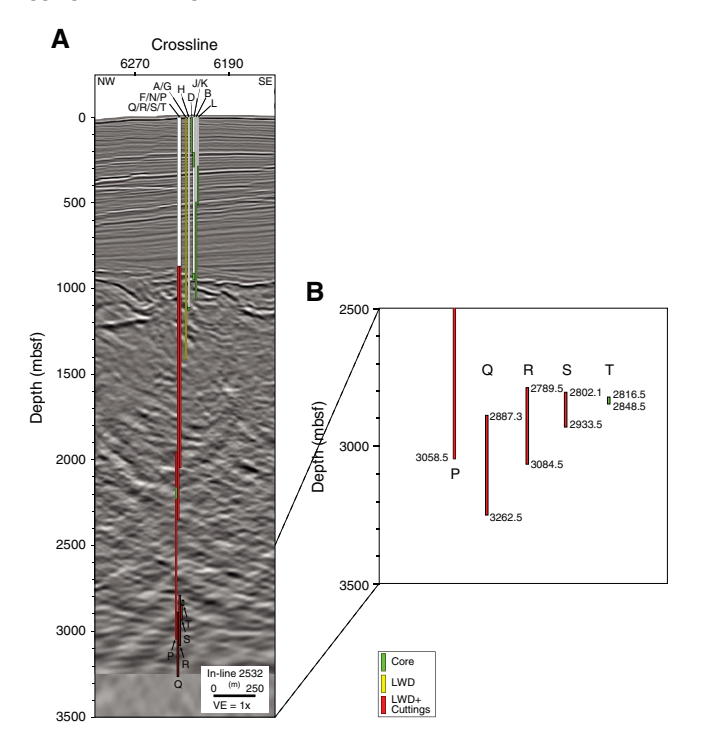
During the expedition, extensive difficulties establishing the sidetracks and advancing the boreholes plagued the operation from the outset and continuously as a series of mitigation strategies were attempted (Figures F4C, F5). A more complete history of the operations appears below (Tables T1, T2). In summary, riser drilling in Hole C0002Q advanced only to 3262.5 mbsf (204 m deeper than Hole C0002P) before it had to be abandoned. Cuttings were obtained from this hole, but only a very basic LWD data set was acquired, including gamma ray and a resistivity log, rather than the full planned suite that was to include resistivity imaging logs and sonic and check shot seismic data. A second sidetrack was established at 2790 mbsf, and Hole C0002R advanced to 3085 mbsf (Figure F5), again with only cuttings and basic logs acquired. Hole C0002S was sidetracked and met a fate similar to that of Hole C0002R, ending at 2933 mbsf. The final sidetrack Hole C0002T was made, and three cores with minimal recovery were collected from 2836.5 to 2848.5 mbsf before riser operations came to an end.

Unfortunately, these technical setbacks resulted in only very modest scientific achievements at Site C0002. New cores were obtained $\sim\!600$ m deeper than any previous cores from Expedition 348 and before. Cuttings and limited logs were obtained from $\sim\!204$ m of new drilling depth but came 2000 m short of the target. No downhole measurements related to in situ stress conditions were obtained.

Scientific results from cuttings, logs, mud gas monitoring, and cores of sidetrack Holes C0002Q–C0002T are reported in this section (Figure **F6A**).

Lithology

We analyzed cuttings from four overlapping holes (Holes C0002Q–C0002T) and three cores from Hole C0002T. The combined depth interval for those samples extends from 2812.5 to 3257.5 mbsf. We found four rock types with gradational lithologic attributes. Fine silty claystone is light gray to gray in color. Its poorly



consolidated cuttings are typically rounded and sticky. Silty claystone is gray to olive-black and more lithified, and its cuttings are angular and fissile. Siltstone shows a higher degree of lithification, and its cuttings are angular. There are two varieties of sandstone: (1) gray, very fine grained, and angular and (2) light gray, fine grained, less consolidated, and more rounded. Silty claystone is the dominant lithology in Holes C0002Q–C0002T, composing 35%–80% of the total cuttings (Figure F6A). All other lithologies are subordinate, and fine silty claystone decreases to minor amounts. Collectively, all sedimentary rocks correlate with Lithologic Unit V as defined during Expedition 348 (Figure F6B; Tobin et al., 2015b).

X-ray diffraction (XRD) shows that clay minerals (smectite + illite + chlorite + kaolinite) are the most abundant mineral constituent, with normalized percentages of ~40-55 wt% (Figure F6A). Proportions change somewhat with grain size; values for quartz and feldspar are about 5-10 wt% larger in handpicked sandstone and siltstone samples, and abundances of total clay minerals in coarser lithologies are smaller by about 10-20 wt%. Calcite is usually below the detection limit by XRD (<1 wt%). When compared to bulk cuttings at corresponding depths from Hole C0002P, we notice a systematic shift toward modestly higher proportions of quartz and feldspar. Those variations in bulk mineralogy are probably a reflection of natural heterogeneity in a steeply dipping succession of interbedded silty claystone, siltstone, and fine sandstone. Overall, X-ray fluorescence (XRF) results exhibit no significant depth-dependent trends in bulk sediment geochemistry except for a slight increase in MgO with depth. The chemical uniformity within and among the individual holes is consistent with relatively homogeneous proportions of rock types.

The depth interval assigned to Lithologic Subunit VB in Hole C0002P is characterized by abundant fine silty claystone and rare sandstone (Tobin et al., 2015b). The facies was interpreted to be a hemipelagic depositional environment punctuated by sporadic fine-grained turbidity currents (Tobin et al., 2015b). The same depth interval in Holes C0002Q–C0002T appears to contain more fine sandstone and siltstone. These deposits are likewise consistent with mostly hemipelagic deposition but contain modestly higher occurrences of silt and fine-sand turbidity currents. The environment of deposition is therefore likely to have been a trench or an abyssal plain seaward of the trench.

Table T1. Drilling summary, Expedition 358.* = hole top is top of whipstock window depth, † = hole top is start depth of kick off from Hole C0002S. BRT = below rotary table, MSL = from mean sea level. — = not applicable. LWD = logging while drilling, MWD = measurement while drilling. (Continued on next page.) **Download table in CSV format.**

			Water depth		Depth (mbsf)		Depth BRT (m)	
Hole	Latitude	Longitude	BRT (m)	MSL (m)	Тор	Bottom	Тор	Bottom
C0002Q*	33°18′30.4200″N	136°38′12.1740″E	1967.5	1939.0	2887.3	3262.5	4854.8	5230.0
C0002R*	33°18′30.4200″N	136°38′12.1740″E	1967.5	1939.0	2789.5	2995.5	4757.0	4963.0
C0002S*	33°18′30.4200″N	136°38′12.1740″E	1967.5	1939.0	2802.1	2933.5	4769.6	4901.0
C0002T [†]	33°18′30.4200″N	136°38′12.1740″E	1967.5	1939.0	2816.5	2848.5	4784.0	4816.0
C0024A	33°02′02.6379″N	136°47′23.9464″E	3870.0	3841.5	0.0	869.0	3870.0	4739.0
C0024B	33°02′00.0000″N	136°47′23.7960″E	3872.0	3843.5	0.0	6.0	3872.0	3878.0
C0024C	33°02′00.0000″N	136°47′23.7960″E	3872.0	3843.5	6.0	7.0	3878.0	3879.0
C0024D	33°02′00.0000″N	136°47′23.7960″E	3872.0	3843.5	7.0	128.0	3879.0	4000.0
C0024E	33°02′00.0000″N	136°47′23.7960″E	3872.0	3843.5	0.0	625.5	3872.0	4497.5
C0024F	33°02′03.9362″N	136°47′23.9726″E	3868.0	3839.5	0.0	731.0	3868.0	4599.0
C0024G	33°02′00.6490″N	136°47′24.1800″E	3871.5	3843.0	0.0	319.5	3871.5	4191.0
C0025A	33°24′05.4600″N	136°20′09.1428″E	2039.5	2011.0	0.0	580.5	2039.5	2620.0

Table T1 (continued).

·	Cores	Advanced	Core recovery		Cored interval	Date			
Hole	(N)	(m)	(m)	(%)	(m)	Start	Finish	Days in hole	
C0002Q*	_	_	_	_	LWD/MWD	17 Nov 2018	14 Dec 2018	27	
C0002R*	_	_	_	_	LWD/MWD	22 Dec 2018	29 Jan 2019	38	
C0002S*	_	_	_	_	LWD/MWD	3 Feb 2019	8 Feb 2019	5	
C0002T [†]	3	12.0	2.49	20.8	2836.5-2848.5	19 Feb 2019	21 Feb 2019	2	
C0024A	_	_	_	_	LWD/MWD	6 Mar 2019	10 Mar 2019	4	
C0024B	1	6.0	7.14	119.0	0.0-6.0	12 Mar 2019	12 Mar 2019	0	
C0024C	1	1.0	1.37	137.0	6.0-7.0	12 Mar 2019	12 Mar 2019	0	
C0024D	14	121.0	98.52	81.4	7.0-128.0	12 Mar 2019	13 Mar 2019	1	
C0024E	12	111.5	51.52	46.2	510.0-621.5	15 Mar 2019	18 Mar 2019	3	
C0024F	0	0.0	0.00	0.0	0.0	18 Mar 2019	21 Mar 2019	3	
C0024G	24	219.5	140.72	64.1	100.0-319.5	22 Mar 2019	25 Mar 2019	3	
C0025A	19	180.5	123.02	68.2	400.0-580.5	26 Mar 2019	29 Mar 2019	3	

Table T2. Summary of operations and significant events, Expedition 358. Download table in CSV format.

Figure F6. A, B. Summary of results, Site C0002. Proportion of lithology is shown next to the cuttings composite section image. GR = gamma ray. VE = vertical exaggeration. LWD = logging while drilling. (Continued on next page.)

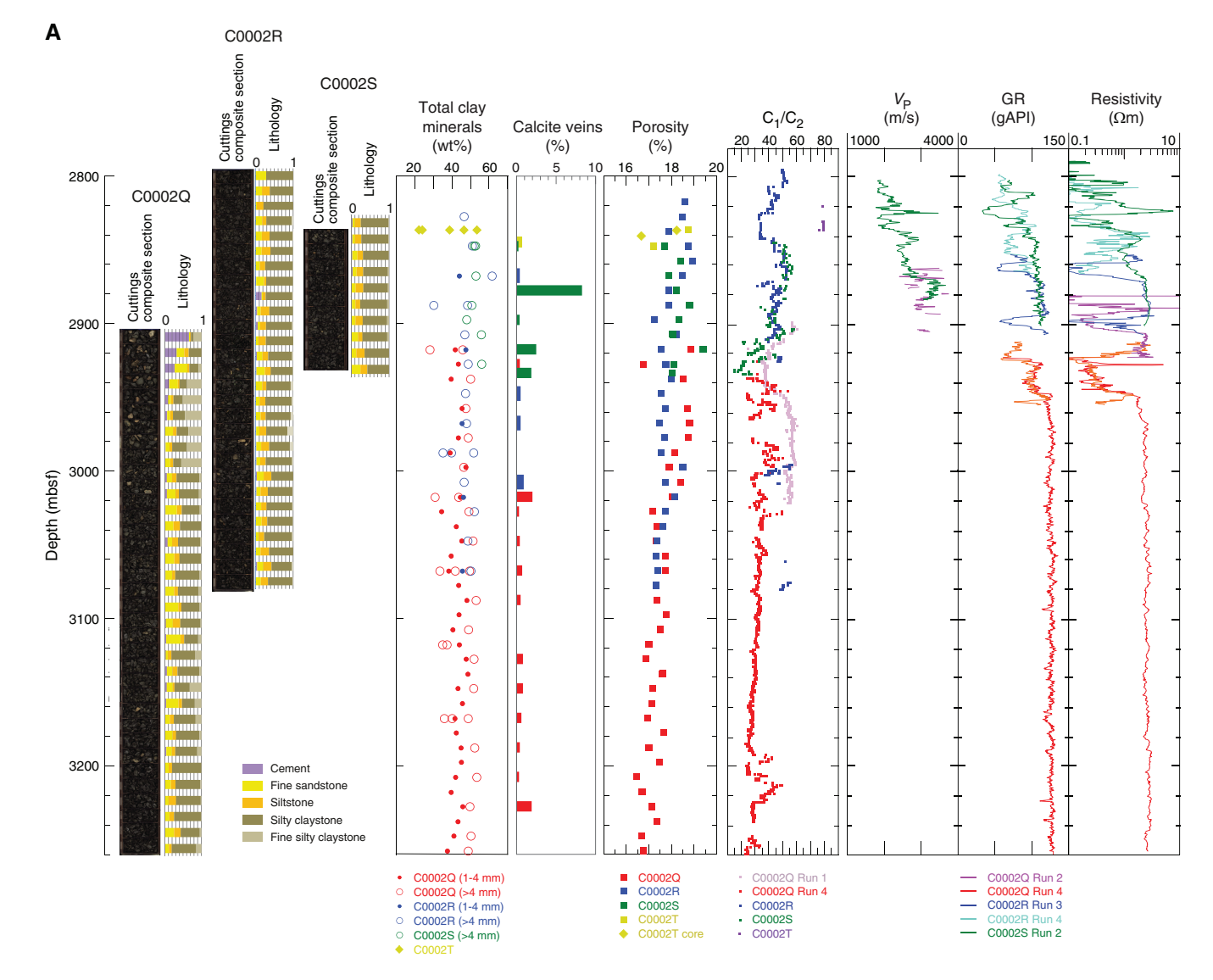
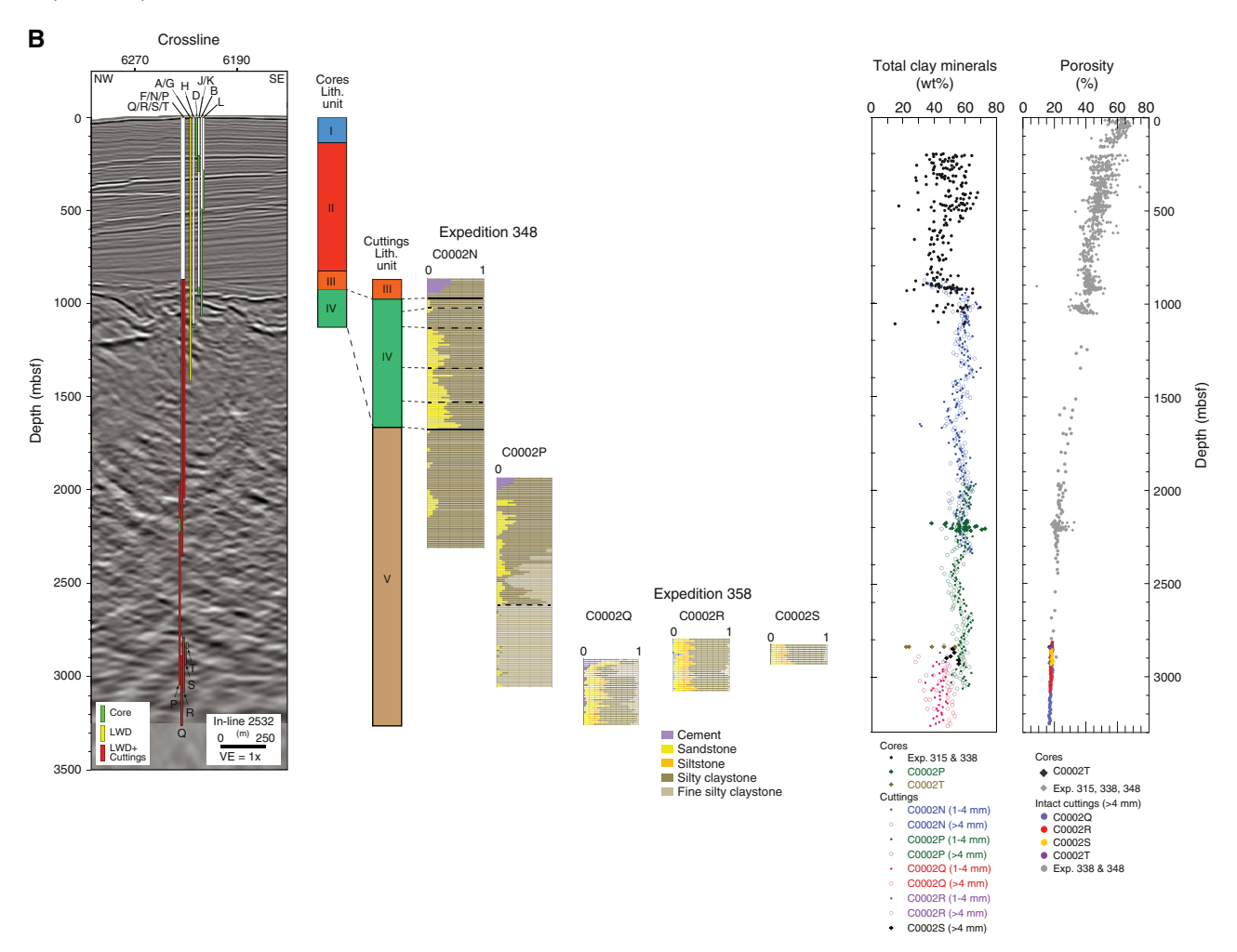


Figure F6 (continued).



Structural geology

Very few identified deformation-related features (<1% of total cuttings exhibit them) occur between 2827.5 and 3262.5 mbsf. Granular and dogtooth calcite veins occur throughout the interval; slickenlines and stepped striae are rare. No scaly fabrics, minor faults, or cataclastic bands were recovered in cuttings from Holes C0002Q–C0002T. The low abundance of deformation structures suggests that the sections of Holes C0002Q–C0002T between 2827.5 and 3262.5 mbsf are weakly deformed.

Mineral veins record different modes and phases of vein formation; crack-seal veins document repeated episodes of extensional fracturing potentially driven by fluctuations in pore fluid pressure or prevailing stress state. Extensional fracturing can be followed by shear deformation as recorded by shear veins and/or slickenlines partially overprinting crack-seal veins and vice versa.

Geochemistry

At Site C0002, mud gas was analyzed from Holes C0002Q–C0002T and compared to earlier drilling in Hole C0002P during Expedition 348 (Tobin et al., 2015b). In addition, cuttings and cores were analyzed for headspace gas content and CaCO₃, total organic carbon, and total nitrogen. Mud gas composition reveals trends similar to the shallower riser drilling during Expedition 348, with decreasing CH_4 and C_1/C_2 ratios downhole, whereas the $\delta^{13}C$ - CH_4

values remain largely between about -50% and about -40%, characteristic of thermogenic gas. Spikes toward higher methane concentrations at $\sim\!2950$, $\sim\!3050$, and $\sim\!3200$ mbsf are accompanied by elevated $\rm H_2$ and $^{222}\rm Rn$ in the mud gas. In contrast, no such elevated concentrations were found in these depth intervals when analyzing the cuttings. All hydrocarbons as well as CO decrease with depth, and n-butane and $\rm H_2$ are particularly low from $\sim\!3050$ mbsf downhole. We suspect that the spikes in real-time mud gas monitoring reflect fluid migration in minor fault zones that would likely not be evident when analyzing cuttings.

Biostratigraphy and paleomagnetism

Preliminary age determination for cuttings from Holes C0002Q–C0002T is based exclusively on the examination of calcareous nannofossils. The abundance and preservation of calcareous nannofossils varies throughout the sequence. Different states of abundance and preservation are recognized even in different pieces from the same cuttings sample. Nannofossil assemblages from the four holes all contain *Reticulofenestra pseudoumbilicus* (≥7 µm), except for a single piece from Slide C of Sample 358-C0002Q-365-SMW (3022.5–3027.5 mbsf). *R. pseudoumbilicus* (≥7 µm) has an age range of 12.8–3.63 Ma with an absence interval of 8.8–7.09 Ma. *R. pseudoumbilicus* together with the presence of *Discoaster prepentaradiatus* (Zones NN9–NN10A; ~10.5–8.3 Ma) in some sam-

ples from the four holes (2847.5–3257.5 mbsf) are likely assigned an age of 10.5–8.8 Ma. An assemblage from Slide C of Sample 365-SMW (3022.5–3027.5 mbsf) that lacks *R. pseudoumbilicus* (\geq 7 μ m) is indicative of an age of 8.8–7.09 Ma.

Radiolarians and foraminifers were also found in Holes C0002Q-C0002S but were not used for age determination because of very rare occurrences. All radiolarians are possibly reworked.

Remanent magnetizations of archive-half sections from Hole C0002T were measured but did not yield useful results regarding magnetic polarity because of poor core quality and recovery.

Physical properties

In Holes C0002Q–C0002T, physical property measurements were conducted mostly on cuttings samples augmented by a few core samples from Hole C0002T. Moisture and density (MAD) measurements show that porosity of handpicked intact cuttings decreases from about 19% at 2800 mbsf to about 17% at 3250 mbsf (Figure F6A), which is in good agreement with the trend found for Hole C0002P during Expedition 348 (Figure F6B). The porosity for bulk cuttings from Hole C0002Q was 10%–20% higher than that of intact cuttings at depths overlapping Hole C0002P, which is again consistent with results from Hole C0002P, but the difference became smaller, or nonexistent, toward the deeper section of Hole C0002Q and in the remaining Holes C0002R–C0002T. The thermal conductivity measured on a core sample from Hole C0002T follows the trend suggested from previous expeditions.

Logging

In Hole C0002Q (logging interval = 2888–3262 mbsf), phase resistivity remains almost uniform over most of the logged interval and ranges between 2 and 3 Ω m (Figure F6A). Gamma ray is slightly more variable, suggesting a mostly uniform lithology with short excursions to lower values that could indicate fine sandy intervals or other minor lithologies. These logging responses fit the characteristics of Logging Subunit Ve identified in the deeper section of

Hole C0002P (Tobin et al., 2015b), suggesting that the entire logged interval belongs to the same subunit.

In Hole C0002Q at 2907–2916 mbsf, borehole failures are observed in a northwest–southeast orientation. The southeastern conductive zone has a larger width (\sim 93°) than the northwestern zone (\sim 61°). Because the southeast and northwest azimuths are approximately equivalent to the upper and lower sides of the deviated borehole, respectively, the wider low resistivity zone in the southeast orientation, or at the top of the hole, indicates that the tool was separated from the upper side of the borehole. In contrast, the narrower low resistivity zone on the northwest, or bottom, side of the hole indicates that the tool was largely in contact with the bottom side of the borehole. Therefore, the narrower low resistivity zone in the northwest is considered to reflect the actual occurrence of the borehole failure.

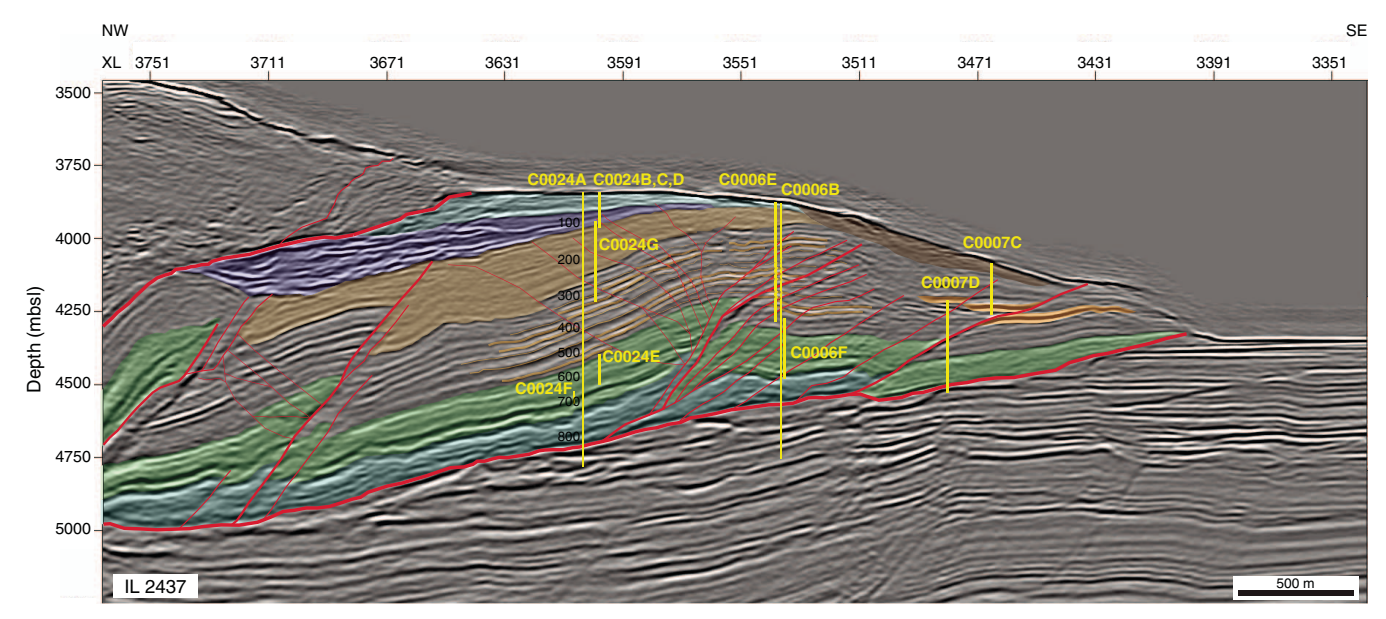
Site C0024

With 28 days remaining in the expedition after the termination of riser operations at Site C0002, drilling was conducted at two alternate contingency sites (Tables T1, T2). Site C0024 is located a few kilometers landward (northwest) of Integrated Ocean Drilling Program Site C0006 in the frontal anticline overlying the frontal thrust (Figure F7). It targeted the hanging wall geology and the main frontal thrust at ~820 mbsf. An LWD hole was drilled into and penetrated the frontal thrust, which is interpreted to be a complex zone of fault strands and imbrication of thrust slices. Coring was attempted in the zone below 500 mbsf, as well as in several shallower intervals, but had to be abandoned because of deteriorating borehole conditions before reaching the main fault zone as identified in log and seismic data. Results from all holes at Site C0024 are summarized in this section (Figure F8).

Lithology

The stratigraphic section at Site C0024 is divided into four lithologic units (Figure F8A). Lithologic Unit I is composed of silty clay

Figure F7. Interpreted seismic depth section of In-line (IL) 2437 in the frontal thrust region with locations of Sites C0024, C0006, and C0007. XL = cross-line. mbsl = meters below sea level. Colored shading = seismic stratigraphic packages, red = faults (bold for major faults), yellow = Site C0006, C0007, and C0024 logging-while-drilling and coring holes.



Deformation Α Chlorinity Total clay C0024B Bedding dip structures dip Porosity (mM) C₁/(C₂+C₃) minerals (wt%) C0024C (°) (%) C0024D 20 40 60 80 30 60 30 60 90 520 600 10³ 104 40 Lith. unit I: 50 C0024G 100 150 Lith. unit II: 200 200 250 300 300 (mpst) Depth (mpst) 350 Depth (400 350 C0024E 500 500 Lith. unit III 550 Lith. unit IV: 600 Coarse to fine sand Silt Silty sand to sandy silt Silty clay to clayey silt C0024B C0024B Normal fault Reverse fault Strike-slip fault C0024D C0024E C0024D C0024E C0024G

Figure F8. Summary of results, Site C0024. A. Core-based results. (Continued on next page.)

to clayey silt. We set the base of Unit I at the top of the uppermost turbidite in Hole C0024B at 3.76 mbsf. No age-diagnostic nannofossils were identified in this interval, so the Holocene age is only inferred. The base of Unit I is a prominent unconformity.

Most of Lithologic Unit II is composed of four lithologies in a continuum of gradational attributes: silty clay to clayey silt, fine to coarse silt, sandy silt to silty sand, and very fine to coarse sand. Scattered beds of volcanic ash are also present. The sand- and silt-rich beds typically display normal size grading, and most such beds are thin (<5 cm). We recorded 1112 event beds, including 30 layers of volcanic ash and 1081 inferred turbidites. A coarsening-upward trend is evident from ~320 to 230 mbsf, and a prominent cluster of thick to very thick beds occurs between ~270 and 230 mbsf. The trend fines upward from ~230 to 58 mbsf and coarsens upward from ~40 mbsf to the seafloor. The overall facies character is consistent with a trench-wedge environment punctuated by frequent influxes by turbidity currents. Most of the accretionary prism at Site C0024 is represented by Lithologic Unit II. Although Unit II yields calcareous nannofossils suggesting an age of 1.34-1.67 Ma in the Matuyama Chron of reversed magnetic polarity, paleomagnetic data indicate dominantly normal magnetic polarity in this unit. Further chronological information is necessary to resolve this inconsistency.

The Lithologic Unit II/III boundary appears to be conformable and is defined by a paucity of sand beds below. Nannofossils dated as 2.06–2.45 Ma reveal no contrast in age across the unit boundary. The dominant lithology in Unit III is silty claystone to clayey siltstone. Minor lithologies include very fine sandstone, siltstone, and volcanic ash or tuff. The mud deposits originated from sustained

hemipelagic settling in an outer trench-wedge setting. Silt beds were deposited from entrained layers of turbidity currents that lapped onto or spilled over the seaward slope of the trench.

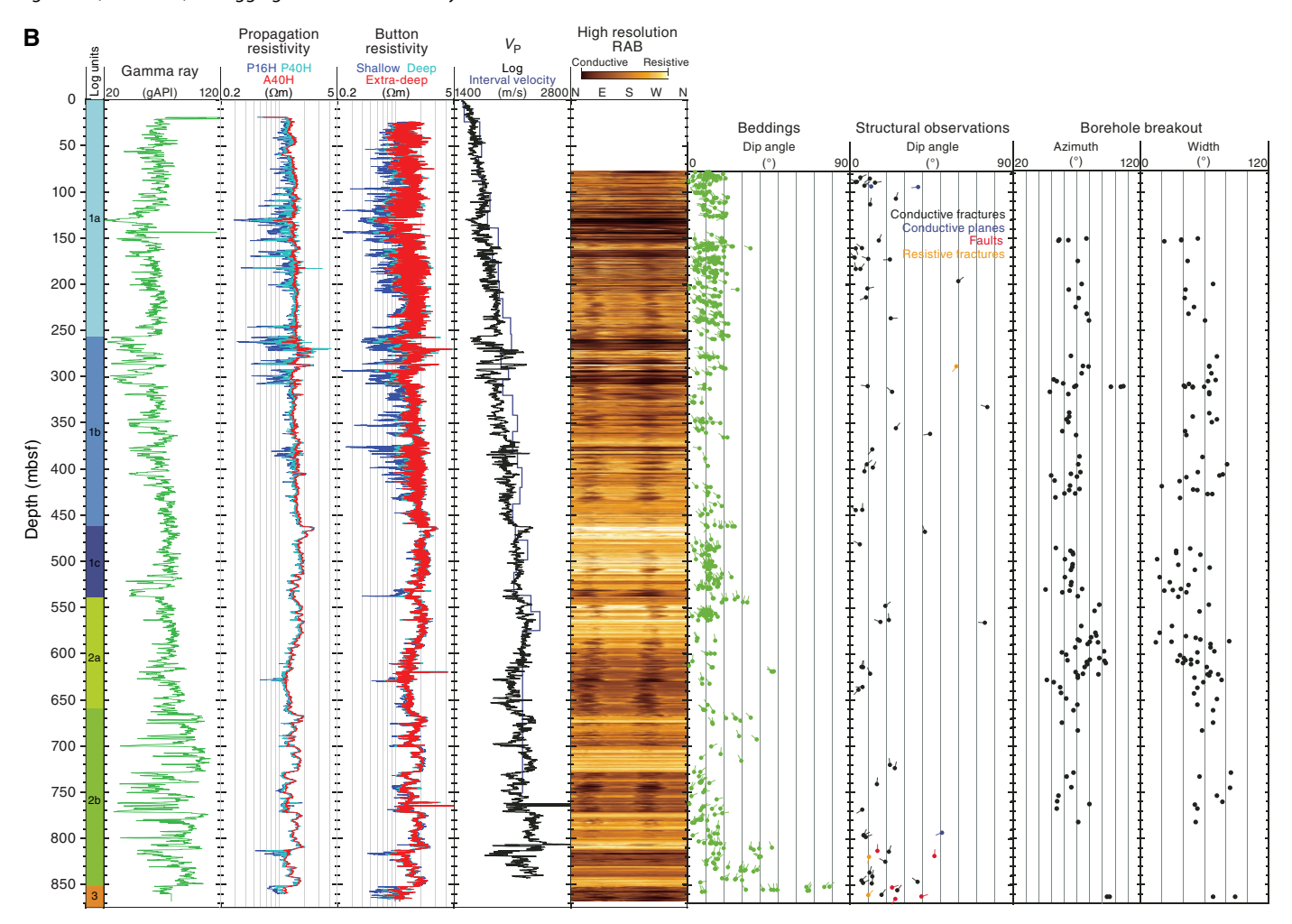
The Lithologic Unit III/IV boundary appears to be conformable and is defined by the last occurrence (moving downsection) of trench-related silty turbidites. Nannofossils reveal no change in age (2.06–2.45 Ma) across the unit boundary. The boundary's position at 555 mbsf matches the top of an anomalous trend in porosity values and the top of a well-defined trend in XRD mineralogy, below which total clay minerals increase with depth (Figure F8A). The dominant lithology is bioturbated silty claystone to clayey siltstone; we also recovered six thin beds of light gray poorly lithified tuff. Sedimentation was dominated by slow hemipelagic settling in an environment that was isolated from sediment gravity flows. These environmental conditions are commonplace across the Shikoku Basin.

Structural geology

Fault (sense unknown) Deformation band Fissility Sediment-filled vein

Bedding dips vary 0° – 30° (38–316 and 510–618.9 mbsf) and are slightly steeper in the shallowest part (\sim 10°–37° at 0–38 mbsf). Steep minor normal faults dipping toward the southwest and northeast are common at 0–38 mbsf, whereas the dip direction shifts toward the northwest and southeast below 100 mbsf. Deformation bands are generally dipping to the northwest or southeast, and healed faults and sediment-filled vein structures are commonly observed at 510–618.9 mbsf. A brecciated zone and a shear zone potentially corresponding to a back thrust that was imaged in the seismic reflection sections (Figure F7) were recovered at 243.5–247 and 295 mbsf, respectively.

Figure F8 (continued). B. Logging data. RAB = resistivity-at-the-bit tool.



Geochemistry

At Site C0024, the chlorinity profile displays two different trends separated by the gap in coring (Figure F8A). In the upper 300 m, the trend in interstitial water (IW) is from a chlorinity value similar to bottom water to one that is 2.5% less fresh at the base of this profile segment. This behavior almost certainly reflects alteration to clay minerals of reactive volcanic matter disseminated in the sediment. Below the coring gap, the trend is reversed so that a 4% freshening occurs over a narrower depth interval from 500 to 620 mbsf. The lower chlorinity profile segment suggests connection at depth with a source of lower chloride water. Another tracer of the deep fluid is the ratio of methane to higher hydrocarbons, the $C_1/(C_2 + C_3)$ ratio. This ratio decreases with depth driven in part by an increase in higher hydrocarbons (Figure F8A). Taken together, these tracers suggest a fluid reservoir at depth sourced from a deeper portion of the prism where clay mineral diagenesis releases freshened waters and thermogenic hydrocarbons are beginning to form. Unfortunately, samples from the décollement and below were not available to characterize the deeper fluids.

Physical properties

At Site C0024, physical property measurements were conducted on core samples collected from 0 to 317.93 mbsf, 510 to 618.13 mbsf, and 652.04 mbsf. MAD measurements on discrete core samples show porosity decreases from about 55%-75% close to the seafloor to about 35% at 550 mbsf (Figure F8A). A sharp increase in porosity to 45%–50% at 550–577 mbsf corresponds to the boundary between Lithologic Units III and IV, marking the transition into the Shikoku Basin sediments underneath. A decrease in magnetic susceptibility from 5×10^{-3} to 1.5×10^{-4} SI measured by the multisensor core logger (MSCL) is also observed around this lithologic boundary, which is consistent with the trend observed at Site C0006 upon entering the upper Shikoku Basin sediments (Expedition 316 Scientists, 2009). P-wave velocity and electrical resistivity measured on discrete samples also show a gradual decrease in velocity and resistivity around the unit boundary, which is consistent with the increase in porosity at the unit boundary. Measured thermal conductivity values generally agree with those measured at Integrated Ocean Drilling Program Sites C0006 and C0011 (Expedition 316 Scientists, 2009; Expedition 333 Scientists, 2012).

Logging

Logging data for Site C0024 were acquired in Hole C0024A with a full bottom-hole assembly (MicroScope, arcVISION, TeleScope, SonicScope, and seismicVISION) in the interval from seafloor to a depth of 869 mbsf (Figure F8B). Good data quality for most of the logged interval allows definition of three logging units with distinct characteristics. Resistivity, gamma ray, and *P*-wave velocity increase

with depth in Logging Unit 1 (0–538.6 mbsf), and then resistivity and *P*-wave velocity show constant trends with some significant negative spikes in Logging Unit 2 (538.6–851.7 mbsf). Logging Unit 3 (851.7 mbsf to TD) is characterized by a significant decrease in resistivity. Both button and propagation resistivity show a large separation of shallow and deep resistivities over this unit, which may be affected by poor borehole conditions.

Bedding planes and fractures can be identified on resistivity images. Bedding dips mainly toward the northwest-northeast with dip angles of ~20° above 809 mbsf. Below 809 mbsf to TD, the overall bedding dips sharply increase with a mean value around 40° and a maximum close to 90° at 851 mbsf. Fractures exhibit various dip angles over the logged interval either to the north-northeast or the north-northwest. At 813 mbsf, a pair of faults dipping 15° and 20° toward the north coincide with a further drop in gamma ray, resistivity, and P-wave velocity values (Figure F9). In addition to the above log response and image observation, a synthetic seismogram using P-wave velocity and vertical seismic profile data indicates that the decrease in P-wave velocity values at ~806 to ~819 mbsf likely corresponds to the interpreted fault reflection in the seismic reflection volume. Our preliminary interpretation is that the onset of deformation at ~806 to ~819 mbsf marks the top of the plate boundary fault zone. Borehole breakouts were also identified on the resistivity images throughout the hole. The orientation of the breakouts is generally consistent at 070°. Between 530 and 630 mbsf, we observed a slight shift in breakout orientation to higher azimuths. A shift in breakout orientation to an azimuth of ~100° is also apparent at 810 mbsf.

Site C0025

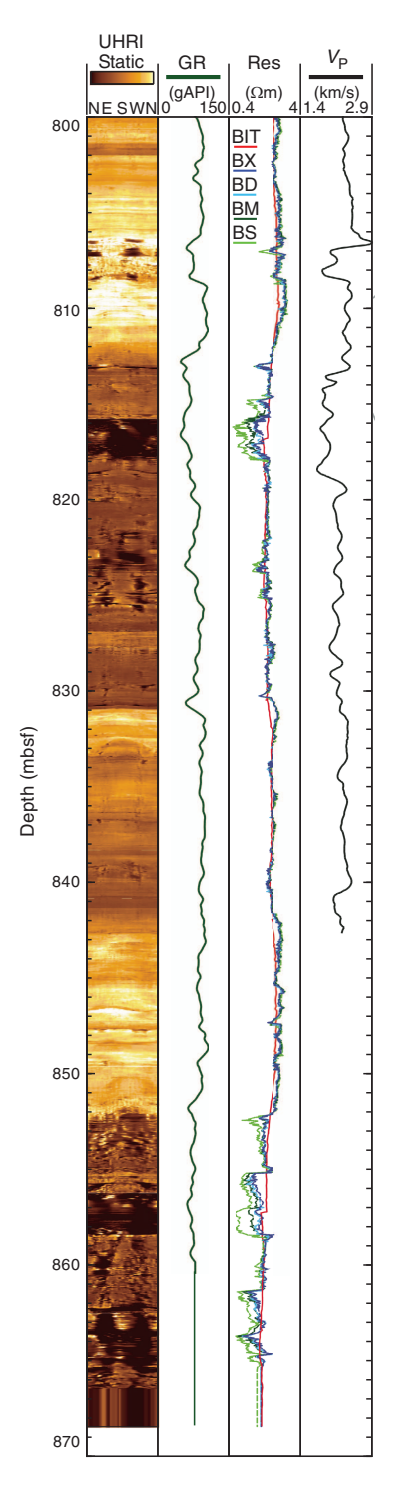
Site C0025, the second riserless contingency site drilled during Expedition 358, was chosen to address questions about the timing of development of the Kumano fore-arc basin and the tectonic history of the inner accretionary wedge. The site is located where the fore-arc basin sediments are underlain by a more deformed domal or antiformal (based on seismic reflection interpretation; Figure F10) formation that is hypothesized to represent either (1) early inner wedge thrust sheet material or (2) diapiric mud rising buoyantly into place. Rotary core barrel (RCB) drilling was carried out after first washing down to 400 mbsf where coring commenced, with the objective of dating and characterizing the lower fore-arc basin and upper underlying wedge to discriminate between these hypotheses and elucidate the basin's tectonic history. Nineteen RCB cores were collected to a TD of 580.5 mbsf, and results from this site are summarized in this section (Figure F11; Tables T1, T2).

Lithology

We documented the lithologic character of 18 cores from Hole C0025A and defined two lithologic units starting at 400 mbsf. The dominant lithology in Lithologic Unit I is mottled silty claystone to clayey siltstone, which we interpret to be hemipelagic mud. Thin interbeds (interpreted to be turbidites) are composed of medium to fine sandstone, silty sandstone, sandy siltstone, and siltstone. The base of Unit I at 441.93 mbsf coincides with the deepest inferred turbidite. The age range of nannofossil assemblages from Unit I is consistent with early Pleistocene deposition. The deposition of Unit I occurred during the initial stages of infilling of the Kumano forearc basin.

Bioturbated silty claystone and clayey siltstone are also common in Lithologic Unit II but are distinguished by a diverse host of secondary attributes: scattered dark green clay-rich bands; concentra-

Figure F9. Logging data from plate boundary fault zone, Site C0024. UHRI = ultrahigh-resolution image, GR = gamma ray, Res = resistivity, BIT = bit, BX = extradeep button, BD = deep button, BM = medium button, BS = shallow button.



tions of organic matter and pyrite; foraminifers, worm tubes, sponge spicules, and *Chondrites–Zoophycos* trace fossils; fine sand laminae; and pumice clasts, thin volcanic ash beds, and irregular ash pods. Glauconite is distinctive as dispersed grains and in concentrated clusters. CaO (from XRF analysis) and calcite (from XRD) values increase significantly in Unit II because of higher propor-

Figure F10. Seismic cross section near Site C0025. Thick section represents cored interval.

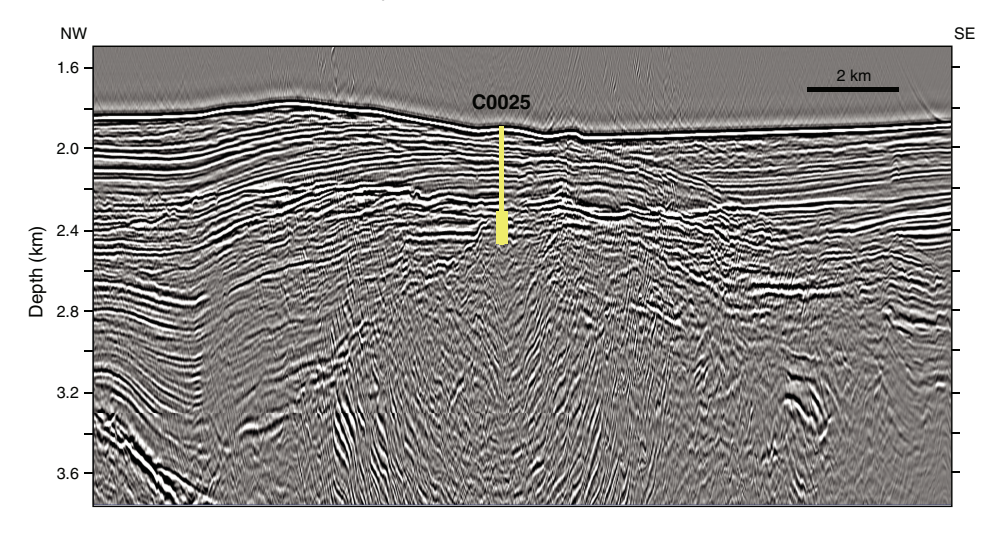
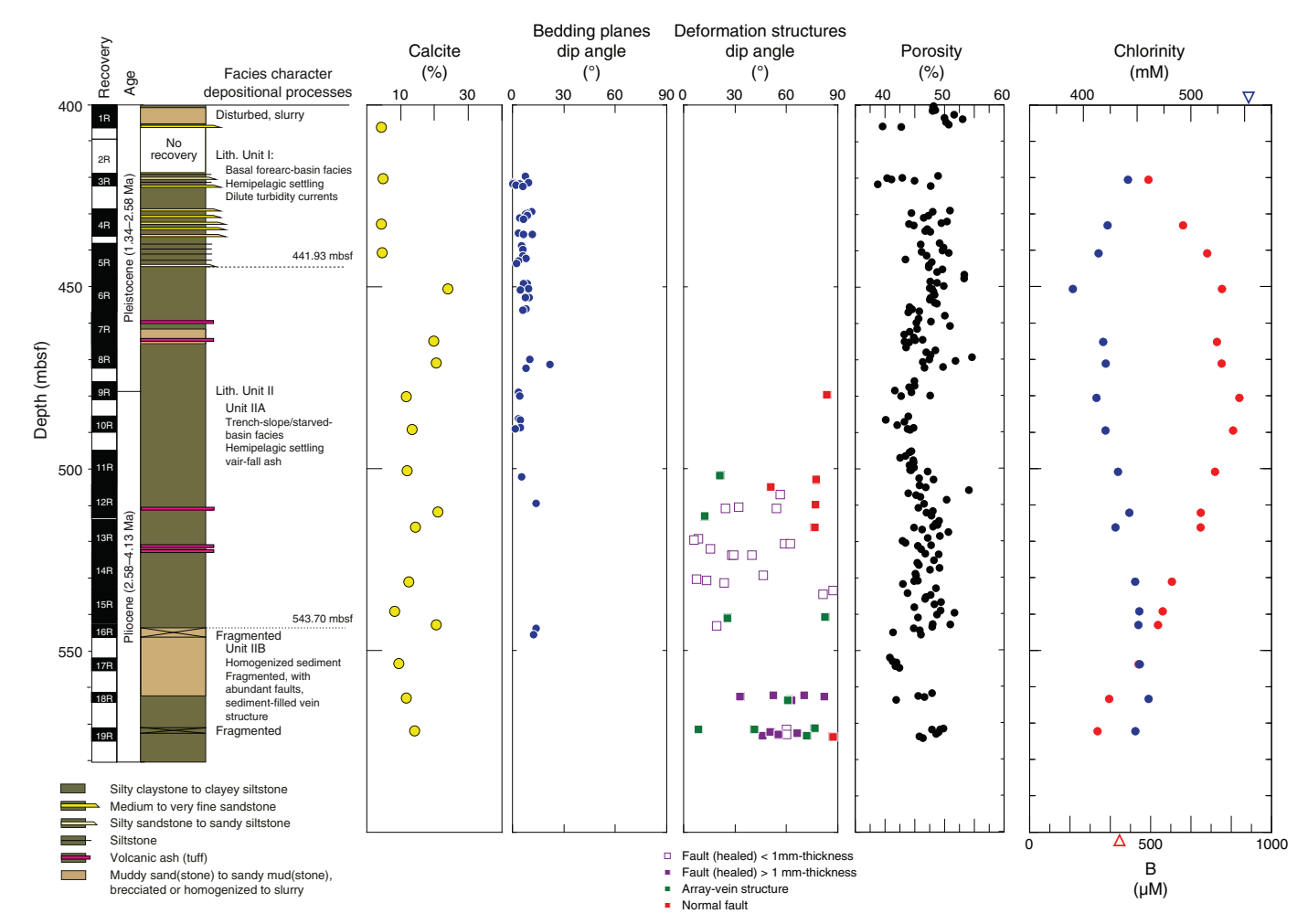


Figure F11. Summary of results, Site C0025. Triangles on chlorinity (blue) and boron (red) plot indicate seawater values.



tions of calcareous nannofossils (Figure **F11**). Nannofossils from Unit II span an age range of late Pliocene to early Pleistocene (1.34–4.13 Ma), and deposition probably occurred in a trench-slope environment with slow sediment accumulation rates. Unusual intervals in Cores 358-C0025A-7R, 16R, and 17R are composed of roughly

equal mixtures of fine sand-, silt-, and clay-sized particles (sandy mudstone to muddy sandstone). Most such examples are unstratified, heavily fragmented, or in extreme cases, reduced to slurry. A provisional subunit boundary at 543.70 mbsf coincides with the top of one such interval.

Structural geology

The structural characteristics at Site C0025 are subhorizontal bedding planes, incohesive normal faults and cohesive (healed) faults, and sediment-filled vein structures. Inclined thick (>1 mm; sometimes >10 cm) healed faults characterized by weak clay mineral orientation and densification are observed in the lower part (Cores 358-C0025A-18R through 19R; 561.5–580.5 mbsf) (Figure F12). Unique sediment-filled vein structures with arrays oriented parallel to and sometimes continuous with the thick faults coexist.

Geochemistry

An important characteristic of the IW at Site C0025 is freshening by 18%–35% as observed in the salinity and chlorinity profiles (Figure F11). The minimum chlorinity value is centered at 450.3 mbsf, which coincides with the depth of the bottom-simulating reflector inferred to represent the base of the gas hydrate stability zone, but low chlorinity extends to at least 572 mbsf. Most dissolved ions at Site C0025 do not greatly vary in concentration with depth. An important exception is boron. Boron concentrations show a broad maximum from 450.3 to 489.2 mbsf with values 2.5 times seawater. High boron coupled with freshened waters is a common signature of mud diapirs located along tectonic strike to the northeast (Kopf et al., 2003). Planned shore-based boron isotope studies may distinguish between processes related to hydrate dissociation or fluid flux from depth causing the observed chemical anomalies.

Physical properties

At Site C0025, physical property measurements were conducted on core samples collected from 400 to 574.34 mbsf. MAD measure-

Figure F12. (A) Photo image logger (MSCL-I) and (B) X-ray computed tomography (CT) images parallel to split core surface (358-C0025A-19R-3, 40–64.5 cm) illustrating sediment-filled veins (green arrows), cohesive healed faults (purple arrows), and a normal fault (red arrows). On X-ray CT images, cohesive healed faults are brighter than surrounding matrix and correspond to higher CT number and density. Normal fault displaces array vein structures (X-ray CT images). Sediment-filled vein structures are generally resolved on X-ray CT images and occur as bright features filled with higher density material. Thinner sediment-filled vein structures by MSCL are not resolved by X-ray CT.



ments on discrete core samples show an overall constant porosity trend scattering between 38.5% and 54.5% (Figure F11). Intervals with sandier formations show relatively lower porosity between 40% and 43%, and the occurrence at 544 mbsf coincides with the boundary between Lithologic Subunits IIA and IIB. Although penetrometer measurements indicate a marked increase in induration at about 465 mbsf, only a slight decrease in porosity (~3%) occurs around this depth. However, a pronounced spike in natural gamma ray count measured by MSCL occurs at this depth because of the presence of glauconite-bearing clasts found in the core. Also, the vertical anisotropy in electrical resistivity (positive when more resistive in the horizontal direction) changes from overall positive to negative at this depth (465 mbsf). Magnetic susceptibility decreases rapidly from 4×10^{-4} to 1×10^{-4} SI between 442 and 450 mbsf, which corresponds to the Lithologic Unit I/II boundary. Measured thermal conductivity values are negatively correlated with porosity and generally agree with those measured on the Kumano Basin sediments at Site C0002 (Expedition 315 Scientists, 2009; Strasser et al., 2014).

Preliminary scientific assessment

Expedition 358 had extraordinarily ambitious scientific goals, representing many firsts in scientific ocean drilling: the first sampling and in situ measurements in a plate boundary fault zone at seismogenic depths of more than 4 km to investigate and document the geology, physical and geochemical properties, and stress conditions of a plate boundary fault zone. Operationally, this required drilling ~2200 m of new depth in an existing cased hole that had already reached ~2900 mbsf, installing and cementing casing along the way, and collecting a suite of LWD logs, cuttings, downhole pressure tests, and 100-200 m of core at selected intervals. Preparation for the potential challenges of geological and stress or fluid pressure conditions in the planned borehole was intense, with several years of planning including the drill well on paper (DWOP) exercise, the implementation of a real-time geomechanics (RTG) team, and external consulting on the mud program and other parameters.

Unfortunately, we were unable to even begin to address the primary scientific objectives because of the operational difficulties encountered continuously throughout the first 4 months of riser drilling. The maximum depth achieved of 3262.5 mbsf is a new record depth for scientific ocean drilling, yet it represents only 10% of the planned advance. Even that 10% is only a partial achievement, as only cuttings and very basic logs (gamma ray and resistivity curves) were acquired to this depth. No LOTs or other downhole measurements relevant to stress and pore fluid pressure were conducted because they were planned for locations just below installed and cemented casing shoes that were not installed. Hole C0002T cores, similarly, are the deepest ever collected, which is an operational achievement; however, they were not taken from a prioritized target zone and yielded little to no new scientific insight. Because Site C0002 riser drilling was the only primary plan for the expedition, the near-complete lack of success in achieving any scientific objectives was a striking disappointment.

Alternative contingency Sites C0024 and C0025 had specific scientific goals that were met with at least partial success. At Site C0024, the objective was to log and sample the frontal décollement zone (shallow plate boundary). The dedicated logging hole appears to have intersected at least the upper fault boundary and as much as 40 m of the fault zone was imaged and logged. It is not clear whether

the base was reached or not. These logs add to a growing global data set of physical properties in active plate boundary fault systems. The high-resolution resistivity image log enabled analyses of borehole breakouts and orientations of planar structures in the plate boundary fault zone and overlying frontal prism. In Holes C0024E and C0024F, coring efforts to reach this zone failed, unfortunately, because of hole stability issues. However, sediments recording the transition between Shikoku Basin and trench fill sediments were successfully recovered from Hole C0024E. Shallow sediments were recovered in cores from Holes C0024B–C0024D and C0024G. The tectonic evolution of the frontal thrust system and strain partitioning between the frontal thrust and splay fault will be elucidated by stratigraphic analysis of these cores and logs, together with the results from Integrated Ocean Drilling Program Sites C0006 and C0007.

At Site C0025, the principal scientific objectives were to obtain age control on the onset of Kumano fore-arc basin filling and the nature of the deformed zone beneath it, testing alternative hypotheses of its formation through tectonic thrust faulting processes or mud diapirism. Coring from 400 to 571 mbsf yielded datable material and possible occurrence for diapiric intrusion of sediments, although there is no involvement of basement rocks. Geochemical and other evidence suggests that older accreted material was not reached in the drilled interval.

In summary, this expedition enjoyed modest successes, mostly during the riserless contingency operations, but unfortunately did not achieve essentially any of the scientific objectives of the primary deep riser drilling plan or really get into position to tackle those objectives. This was not a result of unanticipated geological conditions such as mistaken interpretation or encountering a highly challenging drilling target; rather, the scientific hypotheses were not tested because the primary zone of interest was never reached for operational and engineering reasons.

References

Araki, E., Saffer, D.M, Kopf, A.J., Wallace, L.M., Kimura, T., Machida, Y., Ide, S., Davis, E., and IODP Expedition 365 Shipboard Scientists, 2017. Recurring and triggered slow-slip events near the trench at the Nankai Trough subduction megathrust. *Science*, 356(6343):1157–1160.

https://doi.org/10.1126/science.aan3120

Expedition 314 Scientists, 2009. Expedition 314 Site C0002. In Kinoshita, M., Tobin, H., Ashi, J., Kimura, G., Lallemant, S., Screaton, E.J., Curewitz, D., Masago, H., Moe, K.T., and the Expedition 314/315/316 Scientists, Proceedings of the Integrated Ocean Drilling Program, 314/315/316: Washington, DC (Integrated Ocean Drilling Program Management International, Inc.).

https://doi.org/10.2204/iodp.proc.314315316.114.2009

Expedition 315 Scientists, 2009. Expedition 315 Site C0002. In Kinoshita, M., Tobin, H., Ashi, J., Kimura, G., Lallemant, S., Screaton, E.J., Curewitz, D., Masago, H., Moe, K.T., and the Expedition 314/315/316 Scientists, Proceedings of the Integrated Ocean Drilling Program, 314/315/316: Washington, DC (Integrated Ocean Drilling Program Management International, Inc.).

https://doi.org/10.2204/iodp.proc.314315316.124.2009

Expedition 316 Scientists, 2009. Expedition 316 Site C0006. In Kinoshita, M., Tobin, H., Ashi, J., Kimura, G., Lallemant, S., Screaton, E.J., Curewitz, D., Masago, H., Moe, K.T., and the Expedition 314/315/316 Scientists, Proceedings of the Integrated Ocean Drilling Program, 314/315/316: Washington, DC (Integrated Ocean Drilling Program Management)

International, Inc.).

https://doi.org/10.2204/iodp.proc.314315316.134.2009

Expedition 333 Scientists, 2012. Site C0011. *In* Henry, P., Kanamatsu, T., Moe, K., and the Expedition 333 Scientists, *Proceedings of the Integrated Ocean Drilling Program*, 333: Tokyo (Integrated Ocean Drilling Program Management International, Inc.).

https://doi.org/10.2204/iodp.proc.333.104.2012

Kopf, A., Mora, G., Deyhle, A., Frape, S., and Hesse, R., 2003. Fluid geochemistry in the Japan Trench forearc (ODP Leg 186): a synthesis. *In Suyehiro*, K., Sacks, I.S., Acton, G.D., and Oda, M. (Eds.), *Proceedings of the Ocean Drilling Program, Scientific Results*, 186: College Station, TX (Ocean Drilling Program), 1–23.

https://doi.org/10.2973/odp.proc.sr.186.117.2003

Obara, K., and Kato, A., 2016. Connecting slow earthquakes to huge earthquakes. *Science*, 353(6296):253–257. https://doi.org/10.1126/science.aaf1512

Strasser, M., Dugan, B., Kanagawa, K., Moore, G.F., Toczko, S., Maeda, L., Kido, Y., Moe, K.T., Sanada, Y., Esteban, L., Fabbri, O., Geersen, J., Hammerschmidt, S., Hayashi, H., Heirman, K., Hüpers, A., Jurado Rodriguez, M.J., Kameo, K., Kanamatsu, T., Kitajima, H., Masuda, H., Milliken, K., Mishra, R., Motoyama, I., Olcott, K., Oohashi, K., Pickering, K.T., Ramirez, S.G., Rashid, H., Sawyer, D., Schleicher, A., Shan, Y., Skarbek, R., Song, I., Takeshita, T., Toki, T., Tudge, J., Webb, S., Wilson, D.J., Wu, H.-Y., and Yamaguchi, A., 2014. Site C0002. *In* Strasser, M., Dugan, B., Kanagawa, K., Moore, G.F., Toczko, S., Maeda, L., and the Expedition 338 Scientists, *Proceedings of the Integrated Ocean Drilling Program*, 338: Yokohama (Integrated Ocean Drilling Program).

https://doi.org/10.2204/iodp.proc.338.103.2014

Tobin, H.J., and Kinoshita, M., 2006. NanTroSEIZE: the IODP Nankai Trough Seismogenic Zone Experiment. *Scientific Drilling*, 2:23–27. https://doi.org/10.2204/iodp.sd.2.06.2006

Tobin, H., Hirose, T., Saffer, D., Toczko, S., Maeda, L., Kubo, Y., Boston, B., Broderick, A., Brown, K., Crespo-Blanc, A., Even, E., Fuchida, S., Fukuchi, R., Hammerschmidt, S., Henry, P., Josh, M., Jurado, M.J., Kitajima, H., Kitamura, M., Maia, A., Otsubo, M., Sample, J., Schleicher, A., Sone, H., Song, C., Valdez, R., Yamamoto, Y., Yang, K., Sanada, Y., Kido, Y., and Hamada, Y., 2015a. Expedition 348 summary. *In* Tobin, H., Hirose, T., Saffer, D., Toczko, S., Maeda, L., Kubo, Y., and the Expedition 348 Scientists, *Proceedings of the Integrated Ocean Drilling Program*, 348: College Station, TX (Integrated Ocean Drilling Program).

https://doi.org/10.2204/iodp.proc.348.101.2015

Tobin, H., Hirose, T., Saffer, D., Toczko, S., Maeda, L., Kubo, Y., Boston, B., Broderick, A., Brown, K., Crespo-Blanc, A., Even, E., Fuchida, S., Fukuchi, R., Hammerschmidt, S., Henry, P., Josh, M., Jurado, M.J., Kitajima, H., Kitamura, M., Maia, A., Otsubo, M., Sample, J., Schleicher, A., Sone, H., Song, C., Valdez, R., Yamamoto, Y., Yang, K., Sanada, Y., Kido, Y., and Hamada, Y., 2015b. Site C0002. *In* Tobin, H., Hirose, T., Saffer, D., Toczko, S., Maeda, L., Kubo, Y., and the Expedition 348 Scientists, *Proceedings of the Integrated Ocean Drilling Program*, 348: College Station, TX (Integrated Ocean Drilling Program).

https://doi.org/10.2204/iodp.proc.348.103.2015

Tobin, H.J, Kimura, G., and Kodaira, S., 2019. Processes governing giant subduction earthquakes: IODP drilling to sample and instrument subduction zone megathrusts. *Oceanography*, 32(1):80–93.

https://doi.org/10.5670/oceanog.2019.125

Ujiie, K., and Kimura, G., 2014. Earthquake faulting in subduction zones: insights from fault rocks in accretionary prisms. *Progress in Earth and Planetary Science*, 1:7–37. https://doi.org/10.1186/2197-4284-1-7

Underwood, M.B., and Moore, G.F., 2012. Evolution of sedimentary environments in the subduction zone of southwest Japan: recent results from the NanTroSEIZE Kumano transect. *In Busby, C., and Azor, A. (Eds.), Tectonics of Sedimentary Basins: Recent Advances:* Cambridge, MA (Blackwell Publishing, Ltd.), 310–327.

https://doi.org/10.1002/9781444347166.ch15